Parametric study of the physical properties of hydrate-bearing sand, silt, and clay sediments: 1. Electromagnetic properties

J. Y. Lee,[1] J. C. Santamarina,[2] and C. Ruppel[3]

Received 5 June 2009; revised 31 May 2010; accepted 8 July 2010; published 9 November 2010.

[1] The marked decrease in bulk electrical conductivity of sediments in the presence of gas hydrates has been used to interpret borehole electrical resistivity logs and, to a lesser extent, the results of controlled source electromagnetic surveys to constrain the spatial distribution and predicted concentration of gas hydrate in natural settings. Until now, an exhaustive laboratory data set that could be used to assess the impact of gas hydrate on the electromagnetic properties of different soils (sand, silt, and clay) at different effective stress and with different saturations of hydrate has been lacking. The laboratory results reported here are obtained using a standard geotechnical cell and the hydrate-formed tetrahydrofuran (THF), a liquid that is fully miscible in water and able to produce closely controlled saturations of hydrate from dissolved phase. Both permittivity and electrical conductivity are good indicators of the volume fraction of free water in the sediment, which is in turn dependent on hydrate saturation. Permittivity in the microwave frequency range is particularly predictive of free water content since it is barely affected by ionic concentration, pore structure, and surface conduction. Electrical conductivity (or resistivity) is less reliable for constraining water content or hydrate saturation: In addition to fluid-filled porosity, other factors, such as the ionic concentration of the pore fluid and possibly other conduction effects (e.g., surface conduction in high specific surface soils having low conductivity pore fluid), also influence electrical conductivity.

Citation: Lee, J. Y., J. C. Santamarina, and C. Ruppel (2010), Parametric study of the physical properties of hydrate-bearing sand, silt, and clay sediments: 1. Electromagnetic properties, *J. Geophys. Res.*, *115*, B11104, doi:10.1029/2009JB006669.

1. Introduction

[2] Natural gas hydrates consist of a water lattice that encases low molecular weight guest gas molecules, typically methane. The stability of gas hydrate depends on temperature, pressure, pore water salinity, the composition of the gases trapped in hydrate lattices, and the characteristics of the porous medium [e.g., *Clennell et al.*, 1999]. Pressure, temperature, the state of effective stress, gas hydrate saturation, the arrangement of gas hydrate relative to pore space and soil grains, and sometimes the chemistry of liquid in the pores control the physical properties and behavior of hydrate-bearing sediments. Sample recovery using pressure cores may preserve pressure and sometimes temperature conditions within the stability zone for gas hydrate, but such sampling is always accompanied by a loss of effective stress [e.g., *Yun et al.*, 2007], which fundamentally alters, sometimes irreversibly, many physical properties of hydrate bearing sediments.

[3] Currently, the best means of understanding the properties of natural gas hydrate occurrences under in situ conditions is through the use of borehole logs and geophysical survey data. Yet the interpretation of such field data has to some extent been stymied by the lack of an extensive, internally consistent laboratory data set that can be used for calibrating geophysical parameters as a function of hydrate saturation, soil type, and effective stress. Numerous laboratory studies have used soil samples containing synthetic gas hydrates to investigate the properties of hydrate-bearing sediments [*Cameron et al.*, 1990; *Cortes et al.*, 2009; *Ebinuma et al.*, 2005; *Lee et al.*, 2008; *Priest et al.*, 2005; *Waite et al.*, 2002; *Winters et al.*, 2005; *Yun et al.*, 2005, 2007], but the experiments have been conducted on a variety of soils (or on glass beads [*Spangenberg*, 2001; *Spangenberg and Kulenkampff*, 2006]), with different laboratory devices, and effective stress conditions. Despite these differences, probably the greatest barrier to conducting interexperiment comparisons is the differences in hydrate formation techniques employed by the various researchers, as explored in greater detail by *Lee* [2007], *Santamarina and Ruppel* [2010] and *Yun et al.* [2007].

[4] This paper and *Lee et al.* [2010], coupled with *Yun et al.* [2007] and *Cortes et al.* [2009], provide comprehensive data on the electromagnetic, seismic, thermal conductivity, and strength properties of hydrate-bearing sand, silt, and clay for a range of vertical effective stress and hydrate

[1]Petroleum and Marine Resources Division, Korea Institute of Geoscience and Mineral Resources, Deajeon, South Korea.
[2]School of Civil and Environmental Engineering, Georgia Institute of Technology, Atlanta, Georgia, USA.
[3]U.S. Geological Survey, Woods Hole, Massachusetts, USA.

0148-0227/10/2009JB006669

saturations. For these studies, we have used hydrate formed from dissolved phase, which is the mode of formation that likely dominates most of the world's marine gas hydrate occurrences [*Buffett and Zatsepina*, 2000].

[5] This paper documents the impact of hydrate saturation on the permittivity and electrical conductivity of hydrate-bearing sediments as determined from laboratory experiments conducted within the microwave frequency range (0.2–GHz). This frequency range allows us to operate in reflection mode while running an effective stress controlled test under zero-lateral strain conditions. This frequency range avoids electronic resonance with peripherals, which can occur in the MHz range, and electrode polarization, which determines permittivity at frequencies below ~200 kHz. On the other hand, the permittivity measured at microwave frequencies does not capture spatial and double layer polarizations, factors that affect field-based measurements when tools operate at radio frequencies.

[6] Electrical resistivity, the inverse of electrical conductivity, has long been used to estimate hydrate saturations in sediments of marine and permafrost regions [e.g., *Collett and Ladd*, 2000; *Collett*, 2001; *Hyndman et al.*, 1999] based on applications of Archie's Law [*Archie*, 1942]. In recent years, researchers have also been more broadly applying controlled source electromagnetic (CSEM) surveys to describe the concentration and distribution of gas hydrates in marine sediments [e.g., *Schwalenberg et al.*, 2005, 2008; *Weitemeyer et al.*, 2006]. So far, few drilling studies have been conducted that could verify the inferences about gas hydrate distribution made on the basis of CSEM surveys, whose interpretation also relies on Archie's Law. The systematic laboratory study described here allows us to assess the interpretation of electromagnetic measurements in the context of hydrate-bearing sediments and helps us identify potential pitfalls of using electromagnetic results.

2. Theory

[7] The application of an external electric field to a medium causes charge displacement and polarization in a medium. The resulting current will be out of phase with the applied field. These phenomena are captured by the complex permittivity κ^*

$$\kappa^* = \kappa' - i\kappa'', \tag{1}$$

The real permittivity κ', henceforth referred to simply as permittivity, is a measure of polarization, and the imaginary permittivity κ'' combines electric losses due to polarization and conduction. The effective electrical conductivity σ_{el} [S m^{-1}] for alternating current can be computed from the imaginary permittivity as

$$\sigma_{el} = \kappa'' \varepsilon_o \omega, \tag{2}$$

where ω [s^{-1}] is angular frequency and ε_o is the permittivity of free space [8.854×10^{-12} F m^{-1}].

[8] The permittivity κ' of soil-water mixtures in the microwave frequency range is dominated by the orientational polarization of unfrozen free water molecules, whereas the electrical conductivity σ_{el} of fluid-saturated sediments is governed by pore fluid conductivity (i.e., ionic concentration and mobility in the pore fluid). Both κ' and σ_{el} therefore reflect the characteristics of the unfrozen fluid, modulated by the sediment porosity n and the volume fraction S_w of unfrozen water in the pore space. Surface conduction and double layer polarization, which are both particularly relevant in high specific surface clayey soils, and spatial polarization [e.g., *Santamarina et al.*, 2001] are among the other polarization and conduction processes that may operate in porous media. Double layer and spatial polarizations are manifest at lower (radio) frequencies.

[9] Electromagnetic waves have been used to monitor phase transformations in laboratory studies of hydrates [*Devarakonda et al.*, 1999; *Jakobsen and Folgero*, 1997; *Jakobsen et al.*, 1996; *Lee et al.*, 2008; *Pearson et al.*, 1986; *Yun et al.*, 2005]. When hydrates form, the number of hydrogen bonds increases as water molecules form clusters around the guest molecules, and the polarizability of bonded water molecules vanishes. At the same time, ions dissolved in water are excluded from the hydrate lattice or trapped within intercrystal films during hydrate formation and experience hindered ionic mobility [*Devarakonda et al.*, 1999]. Consequently, the permittivity and the electric conductivity are good indicators of hydrate formation.

3. Methods

[10] The experimental study for this paper was conducted in a zero-lateral strain cell that is instrumented to measure electrical properties, seismic velocities, small-strain stiffness, and zero lateral strain compressibility of hydrate-bearing sediments. The parametric study involves tests on a range of sediment types having various concentrations of hydrate in pores.

3.1. Test Devices

[11] An oedometric cell is used for these tests. The sediment is housed inside a thick walled stainless steel cylinder, and a piston is used to apply controlled vertical effective stress (maximum 3 MPa) while the sediment is maintained under zero-lateral strain conditions. The cell (130 mm outer diameter, 100.6 mm inner diameter, 80 mm height) was designed and built specifically to test hydrate bearing sediments. The specimen is limited to 40 to 50 mm height to ensure optimal geometric and boundary conditions for both oedometric and geophysical measurements.

[12] The cell is instrumented to record the complex permittivity κ^*, shear wave velocity V_S, volume change ε_{vol}, and temperature T (Figure 1). The volume change $\varepsilon_{vol} = \Delta h / h_o$ is estimated from the vertical displacement Δh assuming a one-dimensional deformation of the specimen with starting height h_0. The cell design permits all measurements to be conducted at steady state (constant temperature) as well as during formation and dissociation of synthetic hydrate (changing temperature). A K-type thermocouple mounted through the top cap of the cell is used to monitor the specimen temperature with a precision of 0.1°C. Volume change is determined from the instantaneous vertical position of the top cap using a linear variable displacement transducer (LVDT) with the precision of 2.5×10^{-6} m. The bottom plate houses the coaxial termination probe, which is connected to a computer-controlled network analyzer that measures the complex permittivity κ^* spectrum between 200 MHz and 1.3 GHz. The cell, the loading frame, and

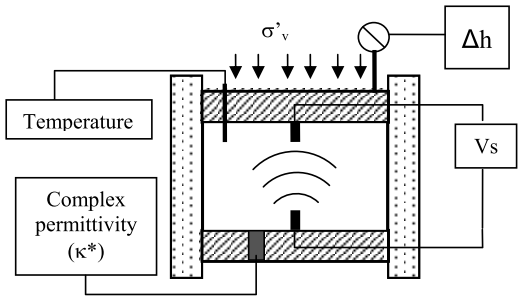

Figure 1. The instrumented odometer cell (zero lateral strain, $\varepsilon_h = 0$) used for this study. The sample occupies the region within the cell walls. Δh refers to the change in height of the specimen (vertical displacement), V_s refers to shear wave velocity measured over the specimen's height, and σ'_v refers to the applied vertical effective stress.

peripheral electronics are operated in a cold room, where the temperature is controlled with a precision of 0.1°C.

3.2. Sediments

[13] The sediments used for this study are sand, crushed silt, precipitated silt, and kaolinite clay. Their index properties are summarized in Table 1. These sediments cover the wide range of grain sizes encountered in natural hydrate-bearing sediments and include proxies for coarse-grained, sand-dominated units with high concentrations of gas hydrate where the first commercial production is likely to occur and for fine-grained, clay-dominated lithologies that characterize some of the classic hydrate provinces (e.g., Blake Ridge [*Paull et al.*, 1996]). The selected quartz sand consists of uniform round particles and has low specific surface. The crushed silica silt has low specific surface and the angular particle shape characteristic of young (poorly worked) sediments. This sediment provides an intermediate grain size between coarse grained and clay-dominated sediments. The precipitated silica flour silt consists of porous aggregations of small particles, making its specific surface much larger than that of crushed silt but with similar particle size. Therefore, the precipitated silt aptly represents dual porosity sediments such as diatom-rich soils sometimes encountered in hydrate bearing provinces [e.g., *Kraemer et al.*, 2000]. The specific surface and effective grain size of the precipitated silt deviate from the trend of increasing specific surface with decreasing grain size in the soils we tested. The kaolinite clay is characterized by platy particles and large specific surface. All sediments are initially dry and include precipitated salts.

3.3. Hydrate Former

[14] Owing to the challenging pressure and temperature stability conditions for methane hydrate, the very low solubility of methane in water, and the difficulty of repeatedly and rapidly forming methane hydrate to the desired saturation from dissolved phase and homogeneously through the sediment, we use tetrahydrofuran (C_4H_8O; THF) as the hydrate former [*Lee et al.*, 2007]. THF is a clear, colorless, low-viscosity liquid with an ether-like odor, high volatility, a low freezing point (−108.5°C), and high miscibility with water. It forms structure II hydrate at a molar ratio of THF-to-water of 1:17. The pressure dependency of THF hydrate stability is low and similar to that of ice. More details about the hydrate formation method and issues related to the use of THF hydrate are explored by *Lee et al.* [2007] and *Yun et al.* [2007].

Table 1. Characteristics of Sediments Used in These Experiments[a]

Sediments	Mean Particle Size D_{50} (μm)	Specific Gravity G_s	Specific Surface S_a (m^2/g)
Sand F110	120	2.65	0.019
Crushed silt	20	2.65	0.113
Precipitated silt	20	2.2	120[b]
Kaolinite clay	1.1	2.6	36[c]

[a]Further details are available from *Yun et al.* [2007].
[b]By N_2 absorption.
[c]By methylene blue.

[15] In addition to deionized water, two other solutions are added to the sediments in this study: (1) a mixture of 21.0% THF and 79.0% water by volume, which forms 100% hydrate saturation (i.e., all the pore fluid becomes hydrate and the hydrate volume fraction in the pore space is S_{hyd} = 1.0), and (2) a mixture of 10.5% THF and 89.5% water by volume, which forms 50% hydrate saturation and leaves behind 50% of the fluid as liquid water (S_{hyd} = 0.5). A mixture of 60.5% THF and 39.5% water by volume also produces S_{hyd} = 0.5 [e.g., *Yun et al.*, 2007] but leaves excess THF after hydrate formation. Of the two mixtures of water and THF that produce S_{hyd} of 0.5 (Table 2), we use the 10.5% THF solution (excess water remaining after hydrate formation) to properly capture the evolution of electrical properties in the S_{hyd} = 0.5 specimens. These specimens require a slow cooling regime characterized by only a small degree of supercooling (temperature maintained close to 0°C) to prevent ice formation.

3.4. Specimen Preparation

[16] Specimens to be tested with S_{hyd} of 0, 0.5, and 1.0 are prepared by first thoroughly saturating the dried soils with the premixed THF and water solution under a ventilation hood. Mixing of the soils and liquid and placement in the cell are conducted carefully to minimize the selective evaporation of THF, whose vapor pressure at 20°C is 160 mm Hg compared to 24 mm Hg for pure water. More details about evaporation control are given by *Yun et al.* [2007].

3.5. Test Procedures and Measurement Protocol

[17] During the experiments, the vertical effective stress σ_v' is applied in four loading steps: 0.01, 0.1, 0.5, and 1.2 MPa.

Table 2. Fluids Added to Saturate Soils for Experiments in This Paper and by *Lee et al.* [2010][a]

Fluids Added[b]	Fluid Composition[c]		After Phase	
	THF (%)	Water (%)	S_{hyd}	Phase
Deionized water	0	100	0.0	all water
10.5% THF solution	10.5	89.5	0.5	hydrate + water
60.5% THF solution[d]	60.5	39.5	0.5	hydrate + THF
21% THF solution	21.0	79.0	1.0	all hydrate

[a]Further details are available from *Yun et al.* [2007].
[b]Dry soils include precipitated salts.
[c]By volume.
[d]Used by *Lee et al.* [2010] only.

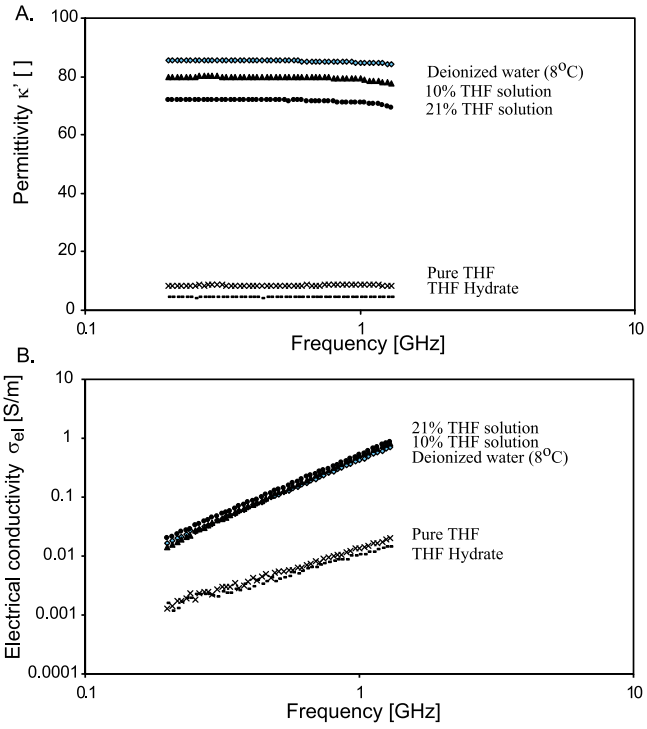

Figure 2. (a) Permittivity and (b) electrical conductivity as a function of frequency for liquids and THF hydrate, without soils present [after *Lee et al.*, 2007].

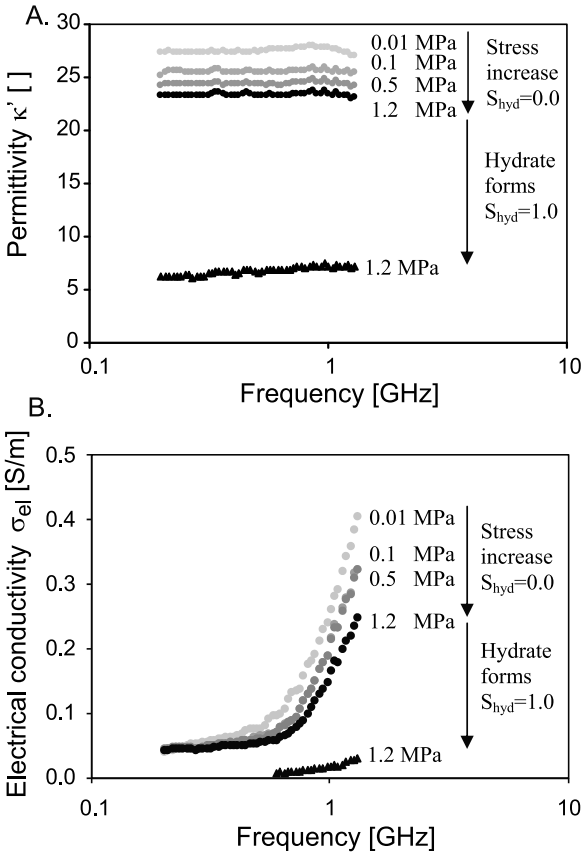

Figure 3. (a) Permittivity and (b) electrical conductivity spectra for different vertical effective stress levels in clay with 21% THF solution as the pore fluid. Also shown is the result obtained after hydrate formation (S_{hyd} = 1.0) at 1.2 MPa.

The stress-temperature history follows this sequence: (1) The external load is applied on the specimen without hydrates; (2) the specimen is completely consolidated, with the end of consolidation determined with Casagrande's log time method [*Terzaghi et al.*, 1996]; (3) the temperature is lowered to induce hydrate formation; (4) the temperature is subsequently increased to cause hydrate dissociation; and (5) a new load is applied. These steps are repeated until the maximum load is reached. After the final loading step, the hydrate-bearing specimen is unloaded to simulate core extraction in the field. Deformation and geophysical properties are measured at each stage in the sequence.

[18] The temperature ranges and cooling methods vary according to the experiments. During hydrate formation, the temperature changes from 10°C to −10°C for specimens with 21% THF solution pore fluid. The temperature is controlled by putting dry ice against the cell wall at constant cold room temperature of 10°C. For specimens with 10% THF solution pore fluid, the specimen temperature is controlled by changing the cold room temperature 1°C every 30 min until phase transformation is reached, typically with some moderate degree of supercooling (−1 to −4°C). Then, the specimen temperature is returned to slightly above 0°C for 24 h to avoid the persistence of any inadvertently formed ice.

4. Results

4.1. Pore Phases

[19] The phases present in sediment pore space largely dominate the electromagnetic response of specimens. It is therefore critical to measure the properties of these pore

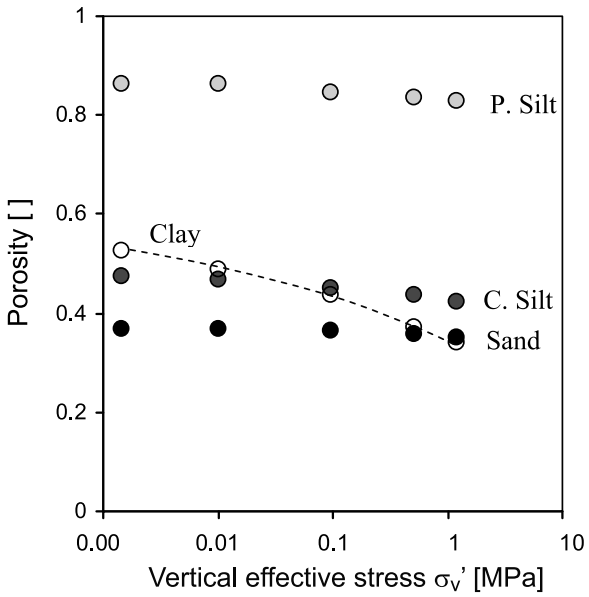

Figure 4. Porosity *n* as a function of vertical effective stress for soils saturated with deionized water. Similar trends and values are noted for soils saturated with THF solutions. The clay specimens (open circles) follow the trend denoted by the dashed line.

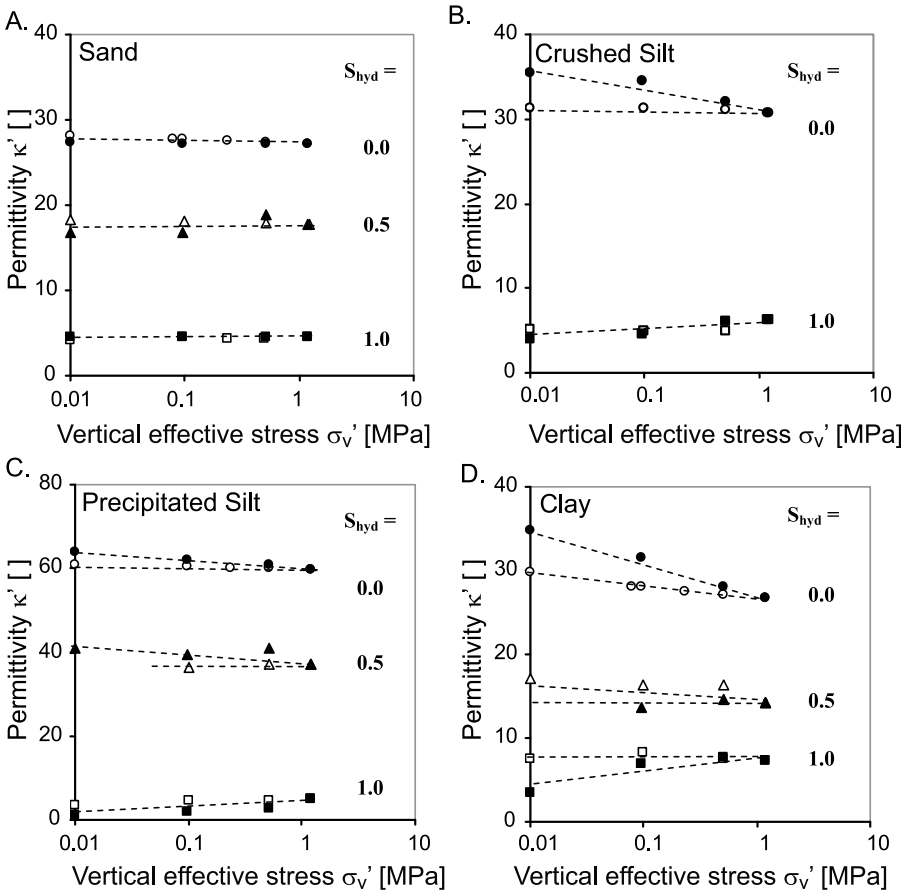

Figure 5. Permittivity at 1 GHz as a function of vertical effective stress for (a) sand, (b) crushed silt, (c) precipitated silt, and (d) clay. Values at 0.2 GHz are similar to those shown here, and there are no significant variations as a function of frequency. The labels to the right of each set of data correspond to S_{hyd} = 0 (circles, with water as the pore fluid), S_{hyd} = 0.5 (triangles, with 10% THF solution as the initial pore fluid), and S_{hyd} = 1 (squares, with 21% THF solution as the initial pore fluid). The numbers in parentheses at the low and high vertical effective stress end-members of the S_{hyd} = 0 curves designate the mean porosity. Solid symbols correspond to the results obtained during loading, while open symbols correspond to unloading of the samples within the hydrate stability field. Note that the permittivity scale is different for the precipitated silt specimens (Figure 5c).

phases before analyzing the properties of bulk samples. Figure 2 shows the spectral response of deionized water, pure THF, THF solutions, and THF hydrate. Owing to the orientational polarization of water, the permittivity κ' of water and THF solutions decreases with frequency and the electrical conductivity σ_{el} increases with frequency. On the other hand, the permittivity and conductivity of THF and THF hydrate are very low and relatively constant with frequency due to the low polarizability of the THF molecule and the hindered orientational polarization of water in hydrate [*Lee et al.*, 2007].

4.2. Spectral Data

[20] Typical spectral permittivity plots gathered for the clay specimen without hydrates at different effective stress levels (0.1 to 1.2 MPa) and with hydrates at 1.2 MPa are shown in Figure 3. The increase in effective conductivity at high frequencies is the most salient feature in these spectral plots and reflects the contribution of free water molecular polarization to AC conduction. As the effective stress increases, κ' and σ_{el} decrease due to the decrease in porosity (i.e., reduced volume fraction of free water). As already documented above, hydrate formation leads to a pronounced decrease in polarizability and conductivity.

4.3. Summary Data

[21] The results presented above underscore the importance of porosity in determining the electrical properties of porous media. To set the stage for the analyses of the electrical measurements obtained for all of the specimens used in our experiments, Figure 4 summarizes porosity values at different effective stress levels for specimens saturated with deionized water. We note similar trends and porosity values for the same sediments saturated with THF solutions, as documented in detail by *Lee* [2007].

[22] Permittivity κ' (measured at 1 GHz) and the electrical conductivity σ_{el} (measured at 0.2 GHz) for all specimens are plotted as a function of vertical effective stress in Figures 5

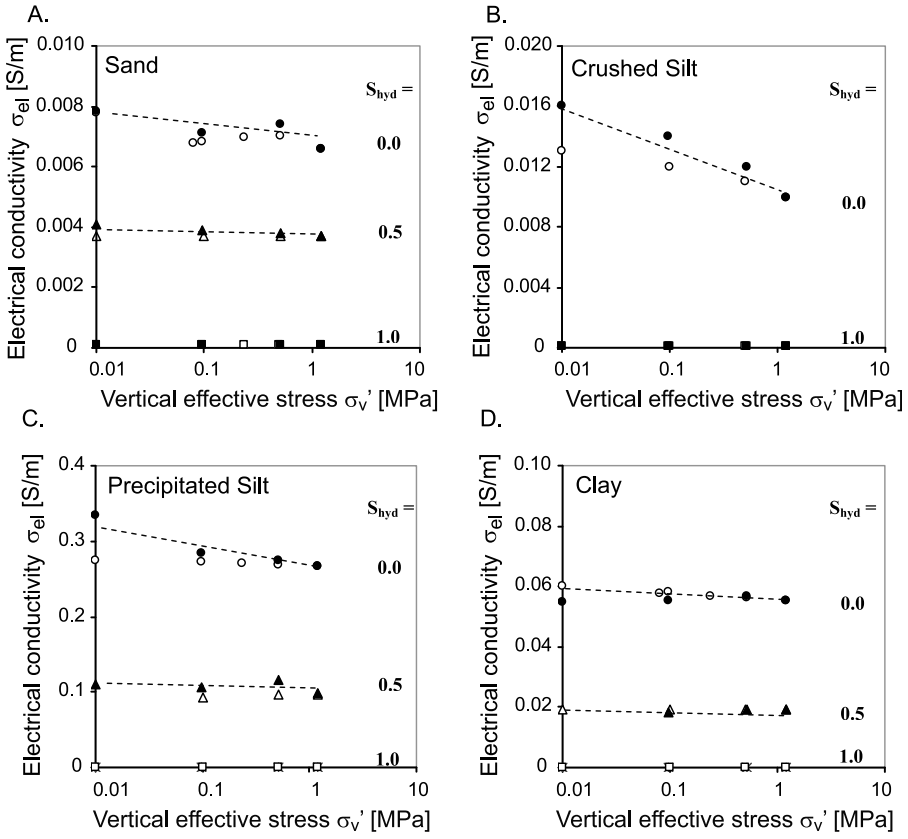

Figure 6. Electrical conductivity at 0.2 GHz as a function of vertical effective stress for (a) sand, (b) crushed silt, (c) precipitated silt, and (d) clay. Symbols and labels the same as in Figure 5.

and 6. Permittivity spectra are almost constant across the measured frequency range, but electrical conductivity data are shown at 0.2 GHz to avoid the contribution of orientational polarization on the effective AC conductivity at higher frequencies. We have already noted that, for $S_{\mathrm{hyd}} = 0$, the permittivity and electrical conductivity decrease as porosity is reduced when the vertical effective stress is increased. The impact of hydrate in pore space is evident for the $S_{\mathrm{hyd}} = 0.5$ specimens; both the permittivity and electrical conductivity are markedly lower once so much of the pore fluid has been transformed into gas hydrate. Once S_{hyd} reaches 1.0, the permittivity is in the range of nonpolarizable materials, and the electrical conductivity has fallen to undetectable values. In contrast to the $S_{\mathrm{hyd}} = 0.0$ specimens, the permittivity of $S_{\mathrm{hyd}} = 1.0$ specimens slightly increases as the vertical effective stress increases and the void ratio decreases. There is a clear explanation for this phenomenon: As the pore volume decreases in response to increasing vertical effective stress, the amount of unfrozen bound water remains constant, but its volume fraction increases, raising the measured permittivity. Porosity does not change significantly during unloading. Consequently, the data show only small changes in permittivity and conductivity.

5. Discussion

[23] Our experimental data confirm that vertical effective stress, porosity, and hydrate saturation are the main factors that govern the electrical properties of hydrate-bearing sediments. In field applications, the porosity derived from the downhole bulk density log represents the space occupied by the fluids and gas hydrates. However, both hydrates and minerals are solid phases, and many physical properties of hydrate-bearing sediments are more closely related to the percentage of porosity that is filled by liquid water. In the absence of gas in the pore space (i.e., volume of gas $V_{gas} = 0$),

$$\frac{V_w}{V_{\mathrm{hyd}} + V_m + V_w} = n\left(1 - S_{\mathrm{hyd}}\right), \tag{3}$$

where V refers to volume and subscripts m, hyd, and w refer to mineral grains, hydrate, and water, respectively. Considering the distinct electrical properties of fluids and solids, we expect the water-filled porosity to exhibit a strong correlation with electrical measurements.

[24] Permittivity values at 1 GHz for all soils and fluids, stress levels, and hydrate saturations are plotted against porosity n in Figure 7. A simple yet robust mixture formula can be written based on the complex refractive index model (CRIM) [*Santamarina and Ruppel*, 2010]:

$$\begin{aligned}\sqrt{\kappa'} &= (1-n)\sqrt{\kappa'_m} + n\left(S_{\mathrm{hyd}}\sqrt{\kappa'_{hyd}} + S_w\sqrt{\kappa'_w}\right) \\ &= (1-n)\sqrt{\kappa'_m} + nS_{\mathrm{hyd}}\sqrt{\kappa'_{\mathrm{hyd}}} + n\left(1 - S_{hyd}\right)\sqrt{\kappa'_w},\end{aligned} \tag{4}$$

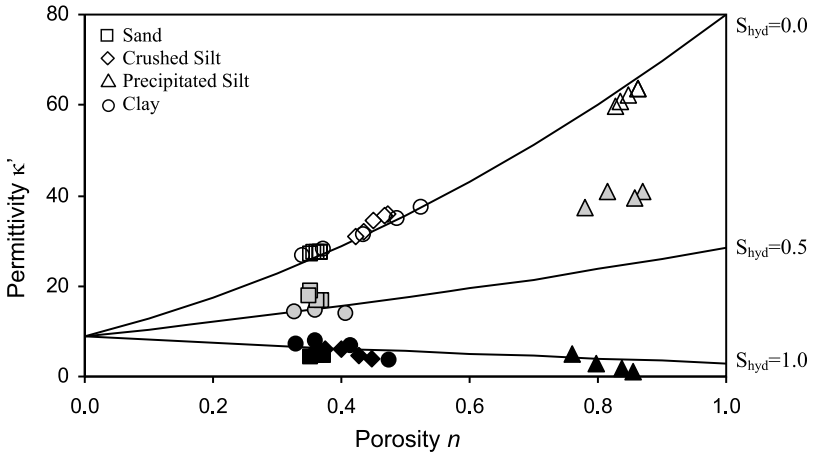

Figure 7. All permittivity results at 1 GHz plotted as a function of porosity. There are no significant spectral features, and permittivity results for 0.2 GHz are similar. Open symbols correspond to S_{hyd} = 0, gray symbols correspond to S_{hyd} = 0.5, and solid symbols correspond to S_{hyd} = 1.0. Symbol shapes are as denoted in the legend. Curves correspond to the complex refractive index model (CRIM) with $\kappa'_m \approx 9$, $\kappa_h' \approx 3$, and $\kappa'_w \approx 80$.

with subscripts the same as in (3). Water-filled porosity, as represented by $n(1 - S_{\mathrm{hyd}})$, has a strong impact on permittivity. Trends predicted from (4) are superimposed on Figure 7. The general agreement between these trends and the data provide support for the use of this simple model. The underprediction of the permittivity for precipitated silt with S_{hyd} = 0.5 may reflect (1) model limitations for these special sediments with internal (dual) porosity; (2) physical effects such as hindered hydrate formation in the small intergrain pores in precipitated silt; or (3) measurement difficulties related to preferential evaporation of THF during specimen preparation. These physical and measurement biases do not affect conductivity measurements, which remain a function of ionic concentration and mobility. Overall, our results show that the permittivity in the microwave frequency range can be used to assess the volume fraction of water, since ionic concentration or soil structure exert only a minor effect on its value.

[25] As noted in section 1, measurements in the low microwave frequency range avoid electrode polarization and instrumentation resonance but fail to capture spatial and double layer polarizations that increase permittivity values measured with field tools operating at lower frequencies. More complex material models are needed to infer the volume fraction of free water when measurements are conducted at radio frequencies.

[26] The electrical conductivity σ_{el} for all sediments is plotted as a function of the water-filled porosity $n(1 - S_{\mathrm{hyd}})$ in Figure 8. We superimpose trends predicted with Archie's semiempirical expression

$$\sigma_{el} = \alpha\sigma_{fl}\left[n\left(1 - S_{\mathrm{hyd}}\right)\right]^{\chi}, \tag{5}$$

where α and χ are fitting parameters. Parameters used in the hydrate literature are in the range $0.7 \le \alpha \le 1.4$ and $1 \le \chi \le 2.8$ [e.g., *Waite et al.*, 2009]. Trends in Figure 8 are shown for two values of the χ exponents, χ = 1 and χ = 2; we fix the α factor at α = 1 to obtain an expression that is consistent with the asymptotic value of conductivity $\sigma_{el} = \sigma_{fl}$ when n = 1 and S_{hyd} = 0. The fluid electrical conductivity, determined by the soluble salts in the sediments, is inferred from the measurements. The results highlight the critical role of pore fluid conductivity σ_{fl} and model parameters (e.g., χ) in the interpretation of the experimental results and underscore the necessity of fully characterizing σ_{fl} if logging data are to be correctly interpreted. When σ_{fl} is not well characterized, α in (5) becomes a surrogate parameter that adjusts to takes into account the impact of pore fluid conductivity. It is also noted that the conductivity for specimens with higher pore fluid conductivity varies more as a function of fluid-filled porosity than when lower conductivity pore fluids are present.

[27] Other conduction phenomena not captured in Archie-type relationships may also contribute to measured conduc-

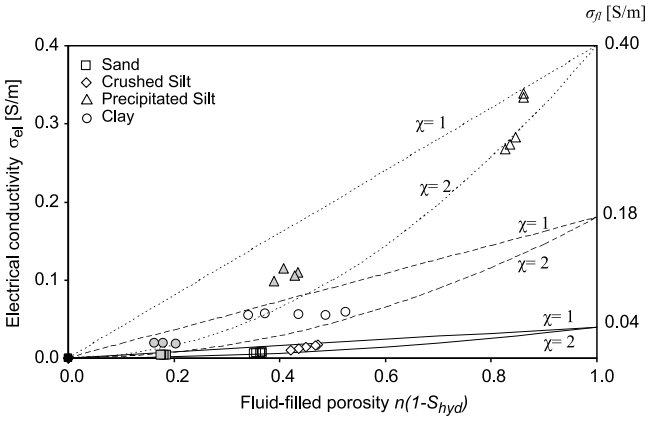

Figure 8. Electrical conductivity as a function of fluid-filled porosity $n(1 - S_{\mathrm{hyd}})$. Trends lines are computed using Archie's expression for three pore fluid conductivities and exponent χ = 1 and χ = 2. Open symbols correspond o S_{hyd} = 0, gray symbols correspond to S_{hyd} = 0.5, and solid symbols (all plot at origin) correspond to S_{hyd} = 1.0. Symbol shapes are as denoted in the legend. The electrical conductivity for specimens with S_{hyd} = 1 (fluid-filled porosity $n(1 - S_{\mathrm{hyd}})$ = 0) falls below detection resolution and is considered immeasurably close to 0.

tivity. In natural settings, these other conduction phenomena could include surface conduction in high specific surface sediments in the presence of very low pore fluid conductivity, conditions that might prevail in some permafrost hydrate settings or when pore waters are freshening due to hydrate dissociation.

6. Conclusions

[28] The formation of hydrates in the pore space of sediments substantially alters the electromagnetic properties of soil-fluid mixtures, producing reductions in permittivity and electrical conductivity. Over the frequency range tested and for the specific hydrate saturations used in the experiments (S_{hyd} = 0, 0.5, and 1), both permittivity and electrical conductivity closely track with water content. Thus, these properties can be used to infer hydrate concentrations in the absence of free gas.

[29] Permittivity in the microwave frequency range is a good indicator of the volume fraction of free water in the sediment and is barely affected by ionic concentration, pore structure, and double layer effects. Consequently, permittivity provides the most reliable geophysical measurement possible of free water content, and a robust estimate of S_{hyd} can be obtained from such data through application of the CRIM model described by equation (4).

[30] Electrical conductivity or resistivity is strongly dependent on both pore fluid conductivity and the fluid volume fraction. Thus, the estimation of fluid-filled porosity from electrical conductivity is directly affected by the selected pore fluid conductivity. The choice of model parameters in Archie-type expressions adds further uncertainty to the inferred saturations. In addition, contributions to conduction not captured in Archie's equation may be important in some settings (e.g., surface conduction in high specific surface soils when the pore fluid conductivity is low).

[31] The interpretation of electromagnetic measurements must take into consideration the frequency range over which data are acquired. Electromagnetic properties in the microwave frequency range are strongly determined by the volume fraction of liquid water and are little affected by pore-scale geometric effects. Consequently, electromagnetic measurements in the microwave frequency range can produce robust estimation of the water-filled porosity regardless of pore structure or hydrate habit in the pore space. Permittivity has the added advantage of not depending on the ionic concentration in the pore fluid.

[32] **Acknowledgments.** This research was initially supported by the Chevron Joint Industry Project on Methane Hydrates under contract DE-FC26-01NT41330 from the U.S. Department of Energy. Additional support was provided to J.C.S. by the Goizueta Foundation at Georgia Tech, to J.Y.L. by KIGAM, and to C. Ruppel by the USGS. We thank W. Waite for comments that improved the manuscript. Any use of a trade, product, or firm name is for descriptive purposes only and does not imply endorsement by the U.S. Government. Any opinions, findings, conclusions, or recommendations expressed herein are those of the authors and do not necessarily reflect the view of the DOE or the USGS.

References

Archie, G. E. (1942), The electrical resistivity log as an aid in determining some reservoir characteristics, *JPT J. Pet. Technol.*, *5*, 1–8.

Buffett, B., and O. Zatsepina (2000), Formation of gas hydrate from dissolved gas in natural porous media, *Mar. Geol.*, *164*, 69–77, doi:10.1016/S0025-3227(99)00127-9.

Cameron, I., Y. P. Handa, and T. H. W. Baker (1990), Compressive strength and creep-behavior of hydrate-consolidated sand, *Can. Geotech. J.*, *27*, 255–258, doi:10.1139/t90-030.

Clennell, M. B., M. Hovland, J. S. Booth, P. Henry, and W. J. Winters (1999), Formation of natural gas hydrates in marine sediments: 1. Conceptual model of gas hydrate growth conditioned by host sediment properties, *J. Geophys. Res.*, *104*, 22,985–23,003, doi:10.1029/1999JB900175.

Collett, T. S. (2001), A review of well-log analysis techniques used to assess gas-hydrate-bearing reservoirs, in *Natural Gas Hydrates, Occurrence, Distribution and Detection*, *Geophys. Monogr. Ser.*, vol. 124, edited by C. K. Paull and W. P. Dillon, pp. 189–210, AGU, Washington, D. C.

Collett, T. S., and J. Ladd (2000), Detection of gas hydrate with downhole logs and assessment of gas hydrate concentrations (saturations) and gas volumes on the Blake Ridge with electrical resistivity log data, *Proc. Ocean Drill. Program, Sci. Results*, *164*, 179–191.

Cortes, D. D., A. I. Martin, T. S. Yun, F. M. Francisca, J. C. Santamarina, and C. Ruppel (2009), Thermal conductivity of hydrate-bearing sediments, *J. Geophys. Res.*, *114*, B11103, doi:10.1029/2008JB006235.

Devarakonda, S., A. Groysman, and A. S. Myerson (1999), THF-water hydrate crystallization: An experimental investigation, *J. Cryst. Growth*, *204*, 525–538, doi:10.1016/S0022-0248(99)00220-1.

Ebinuma, T., Y. Kamata, H. Minagawa, J. Nagao, H. Narita, and R. Ohmura (2005), Mechanical properties of sandy sediment containing methane hydrate, paper presented at Fifth International Conference on Gas Hydrates, Trondheim, Norway, 12–16 June.

Hyndman, R. D., T. Yuan, and K. Moran (1999), The concentration of deep sea gas hydrates from downhole electrical resistivity logs and laboratory data, *Earth Planet. Sci. Lett.*, *172*, 167–177, doi:10.1016/S0012-821X(99)00192-2.

Jakobsen, T., and K. Folgero (1997), Dielectric measurements of gas hydrate formation in water-in-oil emulsions using open-ended coaxial probes, *Meas. Sci. Technol.*, *8*, 1006–1015, doi:10.1088/0957-0233/8/9/009.

Jakobsen, T., J. Sjoblom, and P. Ruoff (1996), Kinetics of gas hydrate formation in w/o-emulsions: The model system trichlorofluoromethane/water/non-ionic surfactant studied by means of dielectric spectroscopy, *Colloids Surf. A*, *112*, 73–84, doi:10.1016/0927-7757(96)03578-9.

Kraemer, L. M., R. M. Owen, and G. R. Dickens (2000), Lithology of the upper gas hydrate zone, Blake Outer Ridge: A link between diatoms, porosity, and gas hydrate, *Proc. Ocean Drill. Program, Sci. Results*, *164*, 229–236.

Lee, J. Y. (2007), Hydrate-bearing sediments: Formation and geophysical properties, Doctoral thesis, 226 pp, Ga. Inst. of Technol., Atlanta.

Lee, J. Y., T. S. Yun, J. C. Santamarina, and C. Ruppel (2007), Observations related to tetrahydrofuran and methane hydrates for laboratory studies of hydrate-bearing sediments, *Geochem. Geophys. Geosyst.*, *8*, Q06003, doi:10.1029/2006GC001531.

Lee, J. Y., J. C. Santamarina, and C. Ruppel (2008), Mechanical and electromagnetic properties of northern Gulf of Mexico sediments with and without THF hydrates, *Mar. Pet. Geol.*, *25*, 884–895.

Lee, J. Y., J. C. Santamarina, and C. Ruppel (2010), Parametric study of the physical properties of hydrate-bearing sand, silt, and clay sediments: 2. Small-strain mechanical properties, *J. Geophys. Res.*, *115*, B11105, doi:10.1029/2009JB006670.

Paull, C. K., R. Matsumoto, and P. J. Wallace, and the Leg 164 Science Party (1996), *Proceedings of the Ocean Drilling Program, Initial Reports*, vol. 164, Ocean Drill. Program, College Station Tex.

Pearson, C., J. Murphy, and R. Hermes (1986), Acoustic and resistivity measurements on rock samples containing tetrahydrofuran hydrates: Laboratory analogs to natural-gas hydrate deposits, *J. Geophys. Res.*, *91*, 14,132–14,138, doi:10.1029/JB091iB14p14132.

Priest, J. A., A. I. Best, and C. R. I. Clayton (2005), A laboratory investigation into the seismic velocities of methane gas hydrate-bearing sand, *J. Geophys. Res.*, *110*, B04102, doi:10.1029/2004JB003259.

Santamarina, J. C., and C. Ruppel (2010), The impact of hydrate saturation on the mechanical, electrical, and thermal properties of hydrate-bearing sand, silts, and clay, in *Geophysical Characterization of Gas Hydrates*, *Geophys. Dev. Ser.*, vol. 14, edited by M. Riedel, E. C. Willoughby, and S. Chopra, pp. 373–384, Soc. Exploration Geophysics, Tulsa, Okla.

Santamarina, J. C., K. A. Klein, and M. A. Fam (2001), *Soils and Waves*, 488 pp., John Wiley, New York.

Schwalenberg, K., E. Willoughby, R. Mir, and R. N. Edwards (2005), Marine gas hydrate electromagnetic signatures in Cascadia and their correlation with seismic blank zones, *First Break*, *23*, 57–63.

Schwalenberg, K., I. Pecher, G. Netzeband, J. Port, and M. Jegen (2008), Marine controlled source electromagnetics on the Hikurangi Margin,

NZ, paper presented at 6th International Conference on Gas Hydrates, Vancouver, B. C., Canada, 6–10 July.

Spangenberg, E. (2001), Modeling of the influence of gas hydrate content on the electrical properties of porous sediments, *J. Geophys. Res.*, *106*, 6535–6548, doi:10.1029/2000JB900434.

Spangenberg, E., and J. Kulenkampff (2006), Influence of methane hydrate content on electrical sediment properties, *Geophys. Res. Lett.*, *33*, L24315, doi:10.1029/2006GL028188.

Terzaghi, K., R. B. Peck, and G. Mesri (1996), *Soil Mechanics in Engineering Practice*, 3rd ed., 604 pp., Wiley-Interscience, New York.

Waite, W. F., B. J. deMartin, S. H. Kirby, J. Pinkston, and C. D. Ruppel (2002), Thermal conductivity measurements in porous mixtures of methane hydrate and quartz sand, *Geophys. Res. Lett.*, *29*(24), 2229, doi:10.1029/2002GL015988.

Waite, W. F., et al. (2009), Physical properties of hydrate-bearing sediments, *Rev. Geophys.*, *47*, RG4003, doi:10.1029/2008RG000279.

Weitemeyer, K., S. Constable, K. Key, and J. Behrens (2006), First results from a marine controlled-source electromagnetic survey to detect gas hydrates offshore Oregon, *Geophys. Res. Lett.*, *33*, L03304, doi:10.1029/2005GL024896.

Winters, W. J., L. Y. Gilbert, D. H. Mason, I. A. Pecher, and W. F. Waite (2005), Effect of grain size and pore pressure on acoustic and strength behavior of sediments containing methane gas hydrate, paper presented at Fifth International Conference on Gas Hydrates, Trondheim, Norway, 12–16 June.

Yun, T. S., F. M. Francisca, J. C. Santamarina, and C. Ruppel (2005), Compressional and shear wave velocities in uncemented sediment containing gas hydrate, *Geophys. Res. Lett.*, *32*, L10609, doi:10.1029/2005GL022607.

Yun, T. S., J. C. Santamarina, and C. Ruppel (2007), Mechanical properties of sand, silt, and clay containing tetrahydrofuran hydrate, *J. Geophys. Res.*, *112*, B04106, doi:10.1029/2006JB004484.

J. Y. Lee, Petroleum and Marine Resources Division, Korea Institute of Geoscience and Mineral Resources, 92 Gwahang-no, Yuseong-gu, Deajeon 305-350, South Korea. (jyl@kigam.re.kr)

C. Ruppel, U.S. Geological Survey, 384 Woods Hole Rd., Woods Hole, MA 02543, USA. (cruppel@usgs.gov)

J. C. Santamarina, School of Civil and Environmental Engineering, Georgia Institute of Technology, 790 Atlantic Dr., Atlanta, GA 30332-0355, USA. (jcs@ce.gatech.edu)